Bone 74 (2015) 83–94

Contents lists available at ScienceDirect

Bone

journal homepage: www.elsevier.com/locate/bone

Original Full Length Article

Histology-directed and imaging mass spectrometry: An emerging technology in ectopic calcification

Domenico Taverna [a,1], Federica Boraldi [b,1], Giorgio De Santis [c], Richard M. Caprioli [d,e], Daniela Quaglino [b,*]

[a] Department of Chemistry and Chemical Technologies, University of Calabria, Arcavacata di Rende, Italy
[b] Department of Life Sciences, University of Modena and Reggio Emilia, Modena, Italy
[c] Department of Medical and Surgical Sciences for Children and Adults, University of Modena and Reggio Emilia, Modena, Italy
[d] Department of Chemistry, Vanderbilt University Medical Center, Nashville, USA
[e] Mass Spectrometry Research Center, Vanderbilt University Medical Center, Nashville, USA

ARTICLE INFO

Article history:
Received 27 September 2014
Revised 24 December 2014
Accepted 7 January 2015
Available online 13 January 2015

Edited by R. Recker

Keywords:
MALDI
Histology
Imaging mass spectrometry
Ectopic calcification
Genetic disease
Connective tissue

ABSTRACT

The present study was designed to demonstrate the potential of an optimized histology directed protein identification combined with imaging mass spectrometry technology to reveal and identify molecules associated to ectopic calcification in human tissue. As a proof of concept, mineralized and non-mineralized areas were compared within the same dermal tissue obtained from a patient affected by Pseudoxanthoma elasticum, a genetic disorder characterized by calcification only at specific sites of soft connective tissues. Data have been technically validated on a contralateral dermal tissue from the same subject and compared with those from control healthy skin. Results demonstrate that this approach 1) significantly reduces the effects generated by techniques that, disrupting tissue organization, blend data from affected and unaffected areas; 2) demonstrates that, abolishing differences due to inter-individual variability, mineralized and non-mineralized areas within the same sample have a specific protein profile and have a different distribution of molecules; and 3) avoiding the bias of focusing on already known molecules, reveals a number of proteins that have been never related to the disease nor to the calcification process, thus paving the way for the selection of new molecules to be validated as pathogenic or as potential pharmacological targets.

Introduction

Calcium and phosphate deposition in soft connective tissues occurs in a number of genetic diseases, in metabolic disorders, such as uremia, hyperparathyroidism and diabetes, or secondary to inflammation or atherosclerosis. Numerous proteins have been identified to be involved in bone calcification as well as in ectopic mineralization, suggesting that an active and dynamic balance of pro-calcifying and anti-calcifying mechanisms takes place in both physiological and pathological calcifications [1]. Nevertheless it is still unclear whether calcification affects particular matrix components in specific organs/tissues, whereas other areas remain unaffected and which molecules/pathways could be targeted for pharmacological approaches. To address these questions, investigations performed so far have looked at the specific expression/localization of already known proteins [2] or have used cell lines and tissue extracts to pick up unknown gene/proteins by means of "omic" techniques [3–5]. However, the major difficulty of these techniques is the ability to analyze a large number of proteins without losing the morphology and the tissue architecture and, even more importantly, to discriminate which proteins belong to normal or to pathologic areas. Therefore, in this study, on-tissue analyses were carried out by Matrix-assisted laser desorption/ionization mass spectrometry (MALDI MS) (profiling and imaging) [6,7] as a consolidated tool for the analysis of biological and clinical tissue samples [8–12]. This approach has several advantages: i) endogenous (locally synthesized by cells) as well as exogenous (derived from the blood stream) molecules can be analyzed directly from the tissue in their native environment, without homogenization, thus preserving spatial relationship of molecules within a specimen; ii) it does not require the use of antibodies; and iii) it can map the expression of hundreds of proteins from a single (8 μm thick) tissue section.

However, MALDI MS, although leading to the detection of a large number of peptides and small proteins (up to 25 kDa), cannot be currently utilized for larger proteins (exceeding 25 kDa). In order to detect also proteins larger than 25 kDa, we have applied a histology-directed mass spectrometry protein identification [13] using hydrogel discs as carriers for the enzyme, thus allowing the digestion to take

* Corresponding author at: Department of Life Sciences, Via Campi 287, 41125 Modena, Italy. Fax: +39 059 2055426.
E-mail address: daniela.quaglino@unimore.it (D. Quaglino).
[1] Equally contributed to the paper.

http://dx.doi.org/10.1016/j.bone.2015.01.004

place directly on discrete tissue areas preserving the relationship between molecular information and tissue architecture.

As the technology advances, the application of MALDI MS as well as of miniaturized hydrogel devices for histology directed on-tissue protein digestion in the clinic will continue to expand, enabling to play a central role in the diagnosis and prognosis of diseases and in the evaluation of patient's therapy.

Therefore, we have combined this MS-based technology in order to investigate skin biopsies from a patient affected by Pseudoxanthoma elasticum, a rare genetic disorder characterized by a progressive calcification occurring in specific areas of soft connective tissues, whereas other regions remain unaffected [14]. Proteomic analyses were performed on mineralized and non-mineralized areas of the same biopsy, and data compared with those from a control healthy tissue.

Material and methods

Tissue specimen collection

The patient was a woman 46 years old affected by Pseudoxanthoma elasticum (PXE). The disease was clinically diagnosed at the age of 15 years by the presence of typical dermal alterations (Fig. 1A) and by ocular angioid streaks. Biomolecular analyses confirmed the clinical diagnosis of PXE revealing two causative missense mutations in the ABCC6 gene: one on exon 12 (c.1553G>A, p.Arg518Gln) and the other on exon 24 (c.3389C>T, p.Thr1130Met).

Control tissue was obtained from a woman 47 years old undergoing elective cosmetic surgical procedures. No connective tissue alterations were present, nor any clinically relevant condition.

Consent was obtained to use these specimens for research purposes in accordance with the Declaration of Helsinki protocol.

After surgery, skin samples were immediately placed in fixatives for morphological analyses or frozen in liquid nitrogen and stored at −80 °C until ready for processing and preparation for mass spectrometry analysis.

Light and electron microscopy

For the demonstration of calcified elastic fibers, skin specimens (approximately 1 cm^3) were routinely fixed in 10% (v/v) formalin in water, dehydrated and embedded in paraffin. Five to seven micron thick sections were collected on glass slides and processed for the von Kossa stain. Briefly, sections were deparaffinized and hydrated, stained for approximately 1 h with 5% (w/v) silver nitrate in water under a UV-lamp, rinsed with water, immersed for 5 min in 5% (w/v) thiosulfate in water and finally observed with a Zeiss Axiophot light Microscope (Jena, Germany).

For ultrastructural observations, specimens were cut in 1 mm^3 fragments and routinely fixed in 2.5% (v/v) glutaraldehyde (Agar Scientific, Stansted, UK) in Tyrode's buffer pH 7.2 (135 mM NaCl, 2.8 mM KCl, 1 mM $MgCl_2$, 2 mM $CaCl_2$, 12 mM $NaHCO_3$, 0.4 mM NaH_2PO_4, 5.5 mM Glucose), postfixed in 1% (v/v) osmium tetroxide (Agar Scientific) in Tyrode's buffer, and dehydrated and embedded in Spurr resin (Agar Scientific). Ultrathin sections (approximately 70–80 nm) were stained with uranyl acetate and lead citrate and observed with a TEM Jeol 2010 (Jeol, Tokyo, Japan).

MS-based techniques: the strategy

A workflow of the analytical approach and technologies we have combined in this study is presented in Fig. 2.

A typical experimental design for MALDI MS protein analysis is made of 3 steps: sample preparation, data acquisition (profiling and imaging) and data processing.

In the *profiling experiment*, the laser beam irradiates each sample spot and ion signals from hundreds of consecutive shots are averaged across the droplet surface generating a mass spectrum. Protein patterns from a discrete number of spots or areas can be compared allowing the analysis of molecules within their native environment.

For *imaging analyses* (MALDI IMS), spectra are recorded for each *x*,*y* coordinate into the mass range 2.5–30 kDa and finally plotted in 2-dimensions for ion density map construction (for each m/z value). Hundreds of protein-specific ion density maps correlated with tissue architecture can be generated. Each pixel (spectrum) contains many proteins and endogenous peptides that are individually displayed as a function of their position and relative intensity within the tissue. Spectra from different regions of interest (i.e. papillary, reticular and mineralized dermis) can be used for statistical analysis.

In a parallel experiment a histology-directed on-tissue protein digestion approach has been applied. Briefly, on-tissue protein digestion was performed using hydrogel discs (1 mm in diameter embedded with trypsin solution) placed on the regions of interest of cryosectioned samples. After digestion, discs were first manually removed from the tissue surface, then properly treated (solvent extracted) and used for LC–MS/MS analysis followed by database search for protein identification (ID).

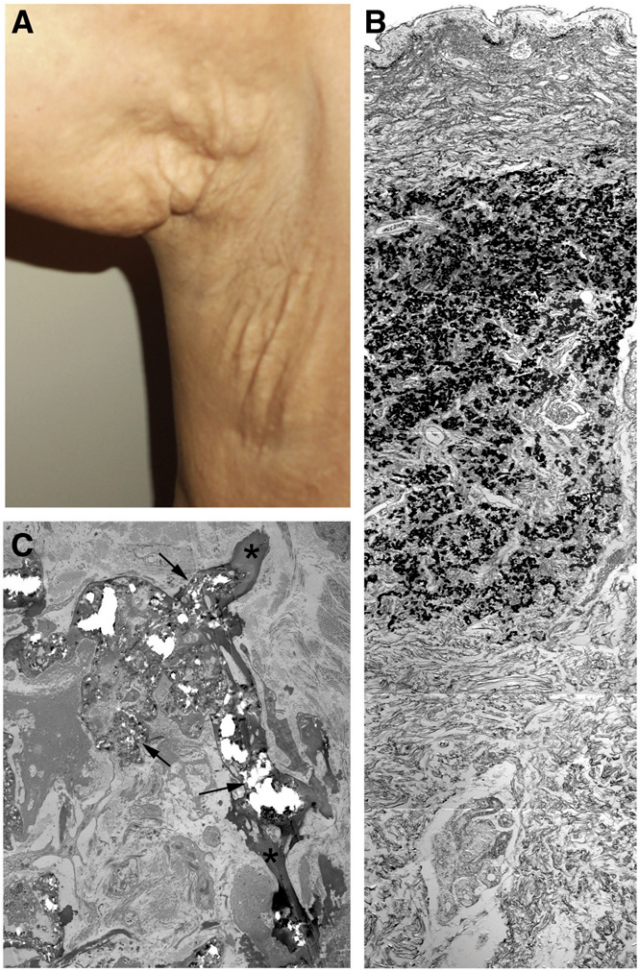

Fig. 1. Clinical phenotype and morphological features observed in PXE. (A–C) Skin laxity (A) is associated to the presence of extended areas of calcification in the reticular dermis as shown after von Kossa staining (B). By ultrastructural analyses (C) it appears that mineral deposits (arrows) are present within elastic fibers, thus altering their typical amorphous structure (asterisk).

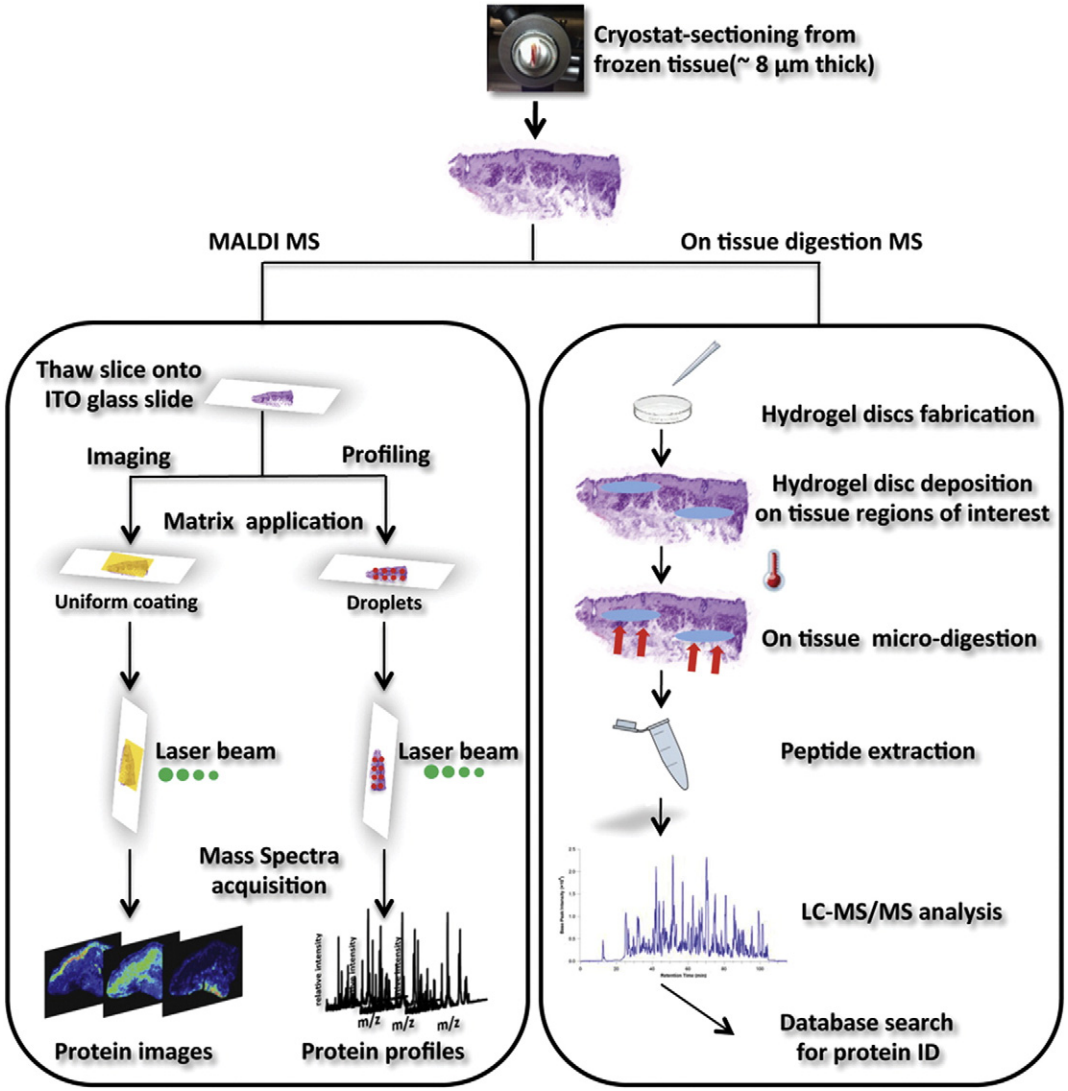

Fig. 2. Scheme of the approach for the analysis of ectopic calcification associated proteins by MALDI MS/IMS and histology-directed on-tissue digestion and protein identification (ID).

Tissue preparation, fixation and contaminant removal

We have recently optimized techniques for IMS analysis of human skin and have used only minor modifications of our published procedures [15,16]. Fresh frozen human skin blocks (approximately 1 cm^3) were sectioned at 8 µm using a cryostat (CM 3050 S, Leica Microsystems GmbH, Wetzlar, Germany) set at −22 °C.

For MS analysis, serial cryosections were collected, mounted on ITO conductive glass slides (Delta Technologies, Stillwater, MN) and allowed to dry at room temperature for 3 min prior to matrix deposition. Each conductive slide was rinsed with Carnoy's (60 mL of ethanol, 30 mL of chloroform, and 10 mL of acetic acid) washing protocol [17] in order to remove interfering species such as salts and lipids [18,19].

For histological orientation, serial cryosections were mounted on glass microscope slides (Fisher Scientific, Pittsburgh, PA) and stained with hematoxylin–eosin and alizarin red, respectively. Briefly, slides were placed in 95% ethanol (v/v) 30 s, purified water 30 s, hematoxylin 120 s, water 15 s, 70% ethanol (v/v) 15 s, 95% ethanol (v/v) 15 s, eosin 60 s, 95% ethanol (v/v) 15 s, 100% ethanol (v/v) 15 s, and xylenes 120 s. Calcium deposition was evaluated by alizarin red staining. Sections were washed at room temperature as follow: xylene (30 s), 90% ethanol (v/v) (30 s), 70% ethanol (v/v) (30 s), purified water (30 s), alizarin red (100 µL, 30 s), acetone (15 s), acetone/xylene (1:1, v/v, 30 s) and finally xylene (3 × 30 s).

MALDI-MS

A crucial step in MALDI MS analyses is represented by the choice of matrix type and of matrix deposition mode (e.g., droplet for profiling by MALDI MS and thin homogenous matrix layer for imaging MALDI MS). Most of the matrices are specific to a mass range or family of compounds, moreover, each matrix type has specific ionization property and this determines differences in the MS spectrum.

Sinapinic acid, for instance, is the matrix of choice for large proteins, whereas α-cyano-4-hydroxy-cinnamic acid (CHCA) is the preferred matrix for peptide mapping.

All MS analyses were performed by an AutoflexSpeed MALDI TOF spectrometer (Bruker Daltonics, Billerica, MA, USA), equipped with a linear TOF (time-of-flight) analyzer, operating in positive polarity, accumulating 500 laser shots per position in the case of the IMS experiment, and 1000 shots per matrix spot in the case of the profiling experiment, at 1000 Hz laser frequency over the m/z range of 2500–30,000 Da. The laser intensity was adjusted before each experiment to yield optimal results. Images were acquired at 50 µm

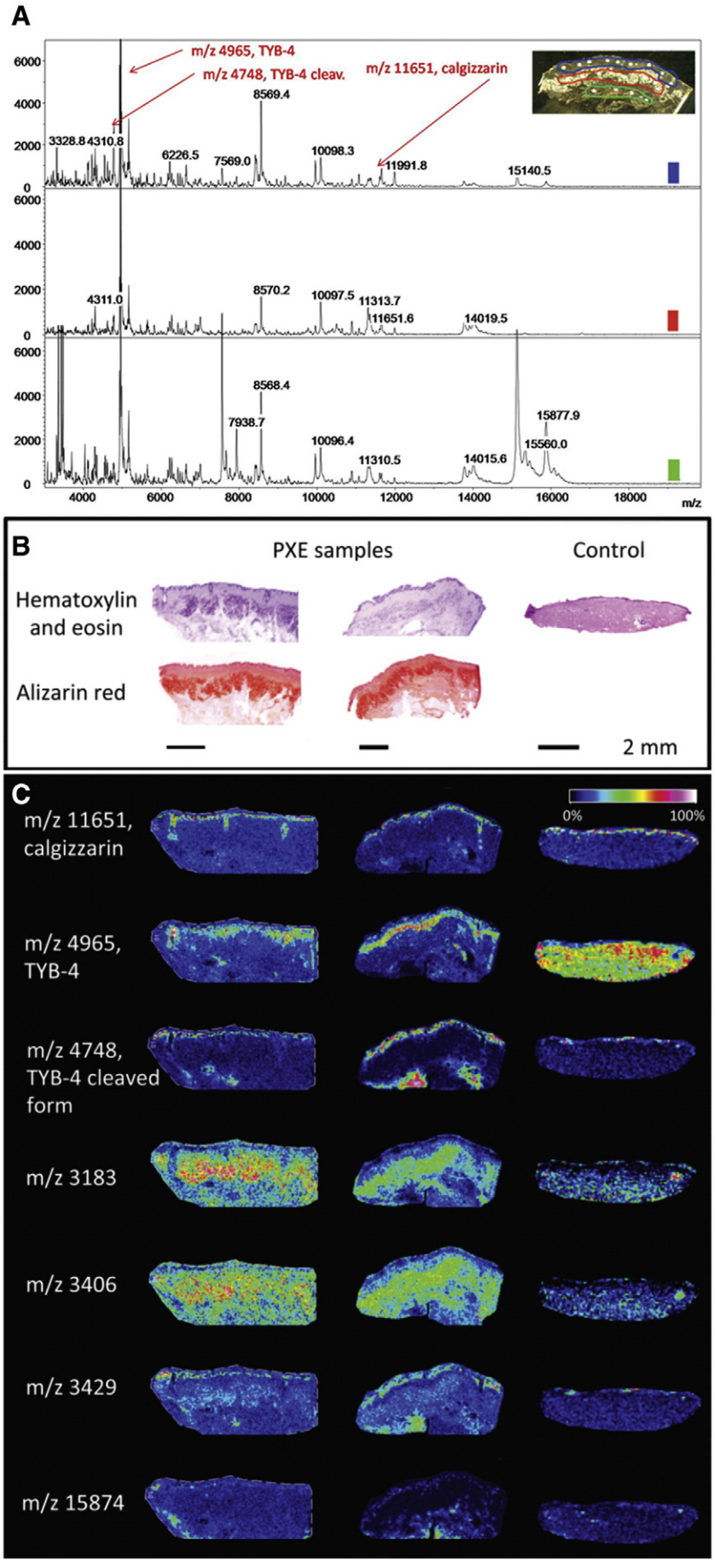
A
m/z 4965, TYB-4
m/z 4748, TYB-4 cleav.
m/z 11651, calgizzarin
8569.4
3328.8
4310.8
6226.5
7569.0
10098.3
11991.8
15140.5
4311.0
8570.2
10097.5
11313.7
11651.6
14019.5
8568.4
7938.7
10096.4
11310.5
14015.6
15877.9
15560.0
m/z
B
PXE samples
Control
Hematoxylin and eosin
Alizarin red
2 mm
C
0%
100%
m/z 11651, calgizzarin
m/z 4965, TYB-4
m/z 4748, TYB-4 cleaved form
m/z 3183
m/z 3406
m/z 3429
m/z 15874

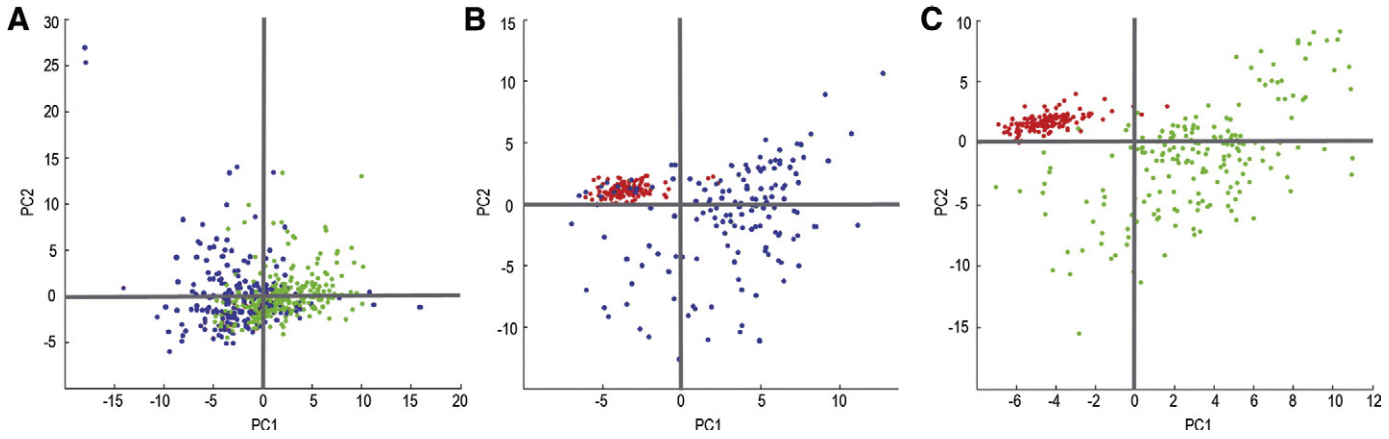

Fig. 4. Principal component analysis (PCA) of spectra from papillary and reticular dermis. (A) In control skin, protein distribution does not show a clear distinction between papillary (blue) and reticular (green) dermis. (B–C) In PXE, spectra from the mineralized area (red) are distinctly separated from those obtained from the papillary (blue) and the non-mineralized reticular (green) dermis.

rastering (spatial resolution). Data acquisition, pre-processing (baseline subtraction of each mass spectrum) and data visualization/process verification were performed using the Flex software suite (FlexControl 3.0, FlexAnalysis 3.0, FlexImaging 3.0) from Bruker Daltonics. Prior to generation of ion density maps, spectra were normalized to the total ion current (TIC) in order to minimize spectrum-to-spectrum differences in peak intensity.

Tissue profiling by MALDI MS

A robotic acoustic droplet ejection system was used for matrix deposition (Portrait 630 reagent multi-spotter, Labcyte, Sunnyvale, CA) [20]. On an 8 μm-cryosection mounted on ITO conductive glass slide, 2 different areas of interest, papillary and reticular dermis (calcified and non-calcified), were targeted for repeated deposition of matrix made of sinapinic acid (20 mg/mL) in 1:1 acetonitrile/trifluoroacetic-acid (Sigma Aldrich, St. Louis, MO, USA) at 0.1% (v/v) aq. that was deposited over a series of 6 iterations at 10 droplets (120 nL) per iteration. After the completion of matrix deposition, slides were immediately returned to vacuum desiccation at room temperature until MS analysis the same day (Fig. 2).

Tissue imaging by MALDI IMS

For imaging mass spectrometry, 8 μm-cryosections mounted on ITO conductive glass slide were coated with a homogenous thin layer of matrix using a sublimation device (Chemglass Life Science, Vineland, NJ, USA). Sublimation of sinapinic acid (300 mg) was carried out at 145 °C, at a pressure of 45 mTorr and, after 15 min, coating became uniform. The aim of this procedure was to allow the mass spectrometer to acquire spectra with a spatial resolution higher than that is possible by an array of evenly spaced spots. Finally, tissue sections were quickly rehydrated at 85 °C for 3 min to allow matrix recrystallization.

Protein identification by LC–MS/MS

Tissue proteins were first digested following a histology-directed in situ digestion method using hydrogel discs for trypsin deposition onto the specific tissue regions of interest (e.g.: dermis, mineralized dermis) [21]. Digestion was performed at 50 °C for 4 h. Hydrogels (1 mm diameter) were re-hydrated for 15 min using 20 μL of 1 μg/mL trypsin (in 100 mM ammonium bicarbonate) and then placed over the tissue region of interest (skin mineralized dermis, adjacent dermis) onto the whole tissue surface guided by the histological features on corresponding serial H&E stained tissue section. The tissue sections were incubated in an oven at 50 °C for 4 h to allow protein digestion. Each hydrogel disc was removed from the tissue section and placed in separate Eppendorf tubes. Peptides imbibed into the microwell hydrogels were extracted by organic (50% acetonitrile/5% formic acid) and aqueous (100 mM ammonium bicarbonate) solvents, a process that was repeated three times. The supernatants collected from each extraction were combined and dried in a centrifugal vacuum concentrator (SPD Speedvac, Thermo Scientific, Waltham, MA, USA). The reconstituted extracts (20 μL, 0.1% (v/v) formic acid) were stored at −20 °C until LC–MS/MS analysis was performed.

The reconstituted extracts were analyzed by a 70 minute data dependent LC–MS/MS analysis as already described [13]. Thus, MS/MS spectra were searched via SEQUEST against a human database (UniprotKB — reference proteome set) that also contained a reversed version for each of the entries [22] (Fig. 2). The criteria used to accept protein identification included the extent of sequence coverage, the number of matched peptides (almost 3 peptides/protein) and a probabilistic score at $p < 0.05$ equivalent to 95% confidence. All protein identifications underwent false discovery rate (FDR) that measures the expected proportion of false positives among the statistically significant findings. The FDR cutoff was set at 0% for all proteins in Scaffold (Proteome Software).

Statistical analysis

Multiple spectra (N = 400) per region of interest (papillary dermis, mineralized dermis, reticula dermis) were selected from the IMS data. Comparisons of different cutaneous regions of interest were conducted using principal component analysis (PCA) to generate classification models based on protein profile patterns. In order to understand how the molecular microenvironment within the mineralized dermis itself can influence adjacent areas, PCA was performed comparing the

Fig. 3. Protein analysis by MALDI MS. (A) Protein profiles were obtained by MALDI MS from papillary (blue trace), mineralized (red trace) and non-mineralized reticular dermis (green trace) in PXE skin. A close inspection of these profiles revealed that, some signals were common to all 3 areas, whereas others were peculiar of a specific region. (B) Optical images of tissue sections after hematoxylin–eosin or alizarin red staining. (C) Seven representative density maps were constructed on the basis of IMS data from an 8 μm thick sagittal section of control healthy and PXE dermis. Protein signals are depicted as color images with red representing the highest relative intensity for each m/z value.

Table 1
List of proteins identified by histology-directed MS.

Short name	Protein name	Accession no.	Short name	Protein name	Accession no.
Proteins identified in the mineralized dermis					
A2AP	Alpha-2-antiplasmin	P08697	HEP2	Heparin cofactor 2	P05546
AEBP1	Adipocyte enhancer-binding protein 1	Q8IUX7	MYPR	Myelin proteolipid protein	P60201
APOE	Apolipoprotein E	P02649	PCOC1	Procollagen C-endopeptidase enhancer 1	Q15113
C1QC	Complement C1q subcomponent subunit C	P02747	PEDF	Pigment epithelium-derived factor	P36955
CAPG	Macrophage-capping protein	P40121	RL4	60S ribosomal protein L4	P36578
CFAI	Complement factor I	P05156	SPP24	Secreted phosphoprotein 24	Q13103
CO6A6	Collagen alpha-6(VI) chain	A6NMZ7	SRPX	Sushi repeat-containing protein SRPX	P78539
FILA	Filaggrin	P20930	THRB	Prothrombin	P00734
H7C2N1	Prothymosin alpha (fragment)	H7C2N1			
Proteins identified in the non-mineralized dermis					
AATM	Aspartate aminotransferase, mitochondrial	P00505	IMMT	Mitochondrial inner membrane protein	Q16891
ACON	Aconitate hydratase, mitochondrial	Q99798	K1C18	Keratin 18	P05783
ACOT2	Acyl-coenzyme A thioesterase 2, mitochondrial	P49753	K22E	Epidermal cytokeratin 2	P35908
ACSL1	Long-chain-fatty-acid–CoA ligase 1	P33121	K2C1B	Keratin 1B	Q7Z794
ADH1B	Alcohol dehydrogenase 1B	P00325	K2C7	Keratin 7	P08729
AK1C2	Aldo-keto reductase family 1 member C2	P52895	K2C8	Keratin 8, type II cytoskeletal	P05787
AL9A1	4-Trimethylaminobutyraldehyde dehydrogenase	P49189	KAD3	GTP:AMP phosphotransferase, mitochondrial	Q9UIJ7
ALDH2	Aldehyde dehydrogenase, mitochondrial	P05091	KAP3	cAMP-dependent protein kinase type II-beta regulatory subunit	P31323
ANXA3	Annexin A3	P12429	LAMA4	Laminin subunit alpha-4	Q16363
ANXA4	Annexin A4	P09525	LAMB2	Laminin subunit beta-2	P55268
ANXA7	Annexin A7	P20073	LAMC1	Laminin subunit gamma-1	P11047
AOC3	Membrane primary amine oxidase	Q16853	LDHB	L-Lactate dehydrogenase B chain	P07195
AT2B4	Plasma membrane calcium-transporting ATPase 4	P23634	LIPS	Hormone-sensitive lipase	Q05469
ATPO	ATP synthase subunit O, mitochondrial	P48047	MARCS	Myristoylated alanine-rich C-kinase substrate	P29966
BLVRB	Flavin reductase (NADPH)	P30043	MDHC	Malate dehydrogenase, cytoplasmic	P40925
CAH1	Carbonic anhydrase 1	P00915	MYL6	Myosin light polypeptide 6	P60660
CALR	Calreticulin	P27797	NCALD	Neurocalcin-delta	P61601
CD44	CD44 antigen	P16070	NUCL	Nucleolin	P19338
DECR	2,4-Dienoyl-CoA reductase, mitochondrial	Q16698	PEBP1	Phosphatidylethanolamine-binding protein 1	P30086
EF2	Elongation factor 2	P13639	PHB	Prohibitin	P35232
EFTU	Elongation factor Tu, mitochondrial	P49411	PIP	Prolactin-inducible protein	P12273
ESYT1	Extended synaptotagmin-1	Q9BSJ8	PLIN1	Perilipin-1	O60240
F213A	Redox-regulatory protein FAM213A	Q9BRX8	PLIN4	Perilipin-4	Q96Q06
FABP4	Fatty acid-binding protein, adipocyte	P15090	PRDBP	Protein kinase C delta-binding protein	Q969G5
FAS	Fatty acid synthase	P49327	PRDX3	Thioredoxin-dependent peroxide reductase, mitochondrial	P30048
FBN1	Fibrillin-1	P35555	RAB5C	Ras-related protein Rab-5C	P51148
FLNB	Filamin-B	O75369	RAP1B	Ras-related protein Rap-1b	P61224
G6PI	Glucose-6-phosphate isomerase	P06744	RBY1B	RNA-binding motif protein, Y chromosome, family 1 member B	A6NDE4
GNAS2	Guanine nucleotide-binding protein G(s) subunit alpha isoforms short	P63092	RL13	60S ribosomal protein L13	P26373
GPDA	Glycerol-3-phosphate dehydrogenase [NAD(+)], cytoplasmic	P21695	S12A2	Solute carrier family 12 member 2	P55011
GRP75	Stress-70 protein, mitochondrial	P38646	SDPR	Serum deprivation-response protein	O95810
HBD	Hemoglobin subunit delta	P02042	SEPT7	Septin-7	Q16181
HMGB1	High mobility group protein B1	P09429	SPB6	Serpin B6	P35237
HNRH1	Heterogeneous nuclear ribonucleoprotein H	P31943	SRBS1	Sorbin and SH3 domain-containing protein 1	Q9BX66
HP183	Heterochromatin protein 1-binding protein 3	Q5SSJ5	TCP4	Activated RNA polymerase II transcriptional coactivator p15	P53999
HYEP	Epoxide hydrolase 1	P07099	TENS1	Tensin-1	Q9HBL0
IDHP	Isocitrate dehydrogenase [NADP], mitochondrial	P48735	TKT	Transketolase	P29401
IGHG3	Ig gamma-3 chain C region	P01860	UBA1	Ubiquitin-like modifier-activating enzyme 1	P22314
ILF2	Interleukin enhancer-binding factor 2	Q12905	XRCC6	X-ray repair cross-complementing protein 6	P12956
Proteins identified in mineralized and non-mineralized dermis (common)					
1433B	14-3-3 protein beta/alpha	P31946	HS90A	Heat shock protein HSP 90-alpha	P07900
1433E	14-3-3 protein epsilon	P62258	HSP71	Heat shock 70 kDa protein 1A/1B	P08107
A1AG1	Alpha-1-acid glycoprotein 1	P02763	HSP7C	Heat shock cognate 71 kDa protein	P11142
A1AT	Alpha-1-antitrypsin	P01009	HSPB1	Heat shock protein beta-1	P04792
A2BHY4	Complement component C4B	A2BHY4	HTTP	Haptoglobin	P00738
A2MG	Alpha-2-macroglobulin	P01023	IC1	Plasma protease C1 inhibitor	P05155
AACT	Alpha-1-antichymotrypsin	P01011	IGHA1	Ig alpha-1 chain C region	P01876
ACTB	Actin, cytoplasmic 1	P60709	IGHG1	Ig gamma-1 chain C region	P01857
ACTC	Actin, alpha cardiac muscle 1	P68032	IGHG2	Ig gamma-2 chain C region	P01859
ACTN1	Alpha-actinin-1	P12814	IQGA1	Ras GTPase-activating-like protein IQGAP1	P46940
ACTN4	Alpha-actinin-4	O43707	ITIH1	Inter-alpha-trypsin inhibitor heavy chain H1	P19827
AHNK	Neuroblast differentiation-associated protein AHNAK	Q09666	K1C10	Keratin 10	P13645
ALBU	Serum albumin	P02768	K1C14	Keratin 14	P02533
ANT3	Antithrombin-III	P01008	K1C19	Keratin 19	P08727

Table 1 (*continued*)

Short name	Protein name	Accession no.	Short name	Protein name	Accession no.
ANXA1	Annexin A1	P04083	K1C9	Keratin 9	P35527
ANXA2	Annexin A2	P07355	K2C1	Keratin 1	P04264
ANXA5	Annexin A5	P08758	K2C5	Keratin 5	P13647
ANXA6	Annexin A6	P08133	K2C6A	Keratin 6A	P02538
APOA1	Apolipoprotein A-I	P02647	KCD12	BTB/POZ domain-containing protein KCTD12	Q96CX2
ARF3	ADP-ribosylation factor 3	P61204	KPYM	Pyruvate kinase isozymes M1/M2	P14618
ARPC4	Actin-related protein 2/3 complex subunit 4	P59998	LAC2	Ig lambda-2 chain C regions	P0CG05
ASPN	Asporin	Q9BXN1	LDHA	L-Lactate dehydrogenase A chain	P00338
ATPA	ATP synthase subunit alpha, mitochondrial	P25705	LMNA	Prelamin-A/C	P02545
ATPB	ATP synthase subunit beta, mitochondrial	P06576	LUM	Lumican	P51884
BGH3	Transforming growth factor-beta-induced protein ig-h3	Q15582	MDHM	Malate dehydrogenase, mitochondrial	P40926
CALD1	Caldesmon	Q05682	MIME	Mimecan	P20774
CALM	Calmodulin	P62158	MOES	Moesin	P26038
CAP1	Adenylyl cyclase-associated protein 1	Q01518	MYH9	Myosin-9	P35579
CAV1	Caveolin-1	Q03135	MYO1C	Unconventional myosin-Ic	O00159
CFAH	Complement factor H	P08603	PDIA1	Protein disulfide-isomerase	P07237
CLH1	Clathrin heavy chain 1	Q00610	PDIA3	Protein disulfide-isomerase A3	P30101
CLUS	Clusterin	P10909	PEPL	Periplakin	O60437
CO1A1	Collagen alpha-1(I) chain	P02452	PGK1	Phosphoglycerate kinase 1	P00558
CO1A2	Collagen alpha-2(I) chain	P08123	PGS1	Biglycan	P21810
CO3	Complement C3	P01024	PGS2	Decorin	P07585
CO3A1	Collagen alpha-1(III) chain	P02461	PLEC	Plectin	Q15149
CO4A2	Collagen alpha-2(IV) chain	P08572	PLSL	Plastin-2	P13796
CO4A4	Collagen alpha-4(IV) chain	P53420	POSTN	Periostin	Q15063
CO6A1	Collagen alpha-1(VI) chain	P12109	PPIA	Peptidyl-prolyl cis-trans isomerase A	P62937
CO6A2	Collagen alpha-2(VI) chain	P12110	PPIB	Peptidyl-prolyl cis-trans isomerase B	P23284
CO9	Complement component C9	P02748	PRDX1	Peroxiredoxin-1	Q06830
COEA1	Collagen alpha-1(XIV) chain	Q05707	PRDX2	Peroxiredoxin-2	P32119
DPYL2	Dihydropyrimidinase-related protein 2	Q16555	PRELP	Prolargin	P51888
DPYL3	Dihydropyrimidinase-related protein 3	Q14195	PROF1	Profilin-1	P07737
E9PCV6	Collagen alpha-3(VI) chain	E9PCV6	PTMS	Parathymosin	P20962
ECHA	Trifunctional enzyme subunit alpha, mitochondrial	P40939	PTRF	Polymerase I and transcript release factor	Q6NZI2
EF1A1	Elongation factor 1-alpha 1	P68104	Q5TCU3	Tropomyosin 2 (Beta)	Q5TCU3
ELN	Elastin	P15502	Q5VU59	Tropomyosin 3	Q5VU59
ENOA	Alpha-enolase	P06733	Q6ZN4A	Tropomyosin 1 (Alpha), isoform CRA_f	Q6ZN40
ENPL	Endoplasmin	P14625	RAB7A	Ras-related protein Rab-7a	P51149
F13A	Coagulation factor XIII A chain	P00488	RLA0	60S acidic ribosomal protein P0	P05388
F5GWP8	Junction plakoglobin	F5GWP8	RLA2	60S acidic ribosomal protein P2	P05387
FIBA	Fibrinogen alpha chain	P02671	ROA2	Heterogeneous nuclear ribonucleoproteins A2/B1	P22626
FIBB	Fibrinogen beta chain	P02675	RS4X	40S ribosomal protein S4, X isoform	P62701
FIBG	Fibrinogen gamma chain	P02679	RS9	40S ribosomal protein S9	P46781
FINC	Fibronectin	P02751	SERPH	Serpin H1	P50454
FLNA	Filamin-A	P21333	SH3L3	SH3 domain-binding glutamic acid-rich-like protein 3	Q9H299
G3P	Glyceraldehyde-3-phosphate dehydrogenase	P04406	SODE	Extracellular superoxide dismutase [Cu–Zn]	P08294
GDIB	Rab GDP dissociation inhibitor beta	P50395	SPTB2	Spectrin beta chain, non-erythrocytic 1	Q01082
GELS	Gelsolin	P06396	SPTN1	Spectrin alpha chain, non-erythrocytic 1	Q13813
GLU2B	Glucosidase 2 subunit beta	P14314	TAGL	Transgelin	Q01995
GRP78	78 kDa glucose-regulated protein	P11021	TBA1B	Tubulin alpha-1B chain	P68363
GSTP1	Glutathione S-transferase P	P09211	TBA4A	Tubulin alpha-4A chain	P68366
H10	Histone H1.0	P07305	TBB4B	Tubulin beta-4B chain	P68371
H12	Histone H1.2	P16403	TBB5	Tubulin beta chain	P07437
H2A1B	Histone H2A type 1-B/E	P04908	TENX	Tenascin-X	P22105
H2B1K	Histone H2B type 1-K	O60814	TERA	Transitional endoplasmic reticulum ATPase	P55072
H32	Histone H3.2	Q71DI3	TLN1	Talin-1	Q9Y490
H4	Histone H4	P62805	TPIS	Triosephosphate isomerase	P60174
HBA	Hemoglobin subunit alpha	P69905	TRFE	Serotransferrin	P02787
HBB	Hemoglobin subunit beta	P68871	VAPA	Vesicle-associated membrane protein-associated protein A	Q9P0L0
HEMO	Hemopexin	P02790	VIME	Vimentin	P08670
HNRPD	Heterogeneous nuclear ribonucleoprotein D0	Q14103	VINC	Vinculin	P18206
HNRPK	Heterogeneous nuclear ribonucleoprotein K	P61978			

mineralized dermis with the adjacent dermis and also with the normal dermis from healthy subject. Protein spectra from the MALDI IMS sequences were compared. PCA was performed because this is a statistical method commonly used to reduce the dimensionality of a multivariate data set to lower dimensions while retaining most of the information by displaying and ranking its variance within a data set. The PCA transforms the original coordinate system (peaks) into the new coordinate system (PC). The new coordinates are called principal components or PCs; so, the first PC (PC1) points in the direction of the highest variance, while the second PC (PC2) points in the direction of the second highest variance. This statistical tool was used to generate classification models based on protein profile patterns. These data were used to confirm the existence of two disparate sub-regions within the dermis in Pseudoxanthoma elasticum disorder affected subjects. The same statistical analysis was

carried out for the papillary and reticular dermis from a healthy subject. Statistical analyses were carried out using ClinProTools software from Bruker (Bruker Daltonics, Billerica, MA, USA).

Functional analysis

To discover the Gene Ontology (GO) categories with significantly enriched protein numbers, the MS identified proteins were processed by the DAVID (Database for Annotation, Visualization and Integrated Discovery) bioinformatics resource v. 6.7, freely available at http://david.abcc.ncifcrf.gov. The significance of "protein"-term enrichment was assured by a modified Fisher's exact test with a p value < 0.01. The protein list was also functionally evaluated applying the UniProtKB/Gene Ontology/Biological Process data processing (http://www.uniprot.org/).

The list of gene IDs of the differentially expressed spots identified were used to perform functional analysis with DAVID 6.7. The list of gene IDs was loaded into the online tool (http://david.abcc.ncifcrf.gov/) clicking on Functional annotation clustering and selecting *gene ID* as identifier and *gene list* as list type. After submission of the list, functional classification was performed on the basis of Gene Ontology.

STRING 9.1 network analysis

Possible connections among identified proteins were analyzed by a protein and gene network software. For each protein, UniProtKB entry numbers and related gene names were acquired in UniProtKB and used for network generation by the use of STRING 9.1 (http://www.string-db.org/) [23,24]. The UniProtKB entry numbers were inserted into the input form as "multiple proteins" and "*Homo sapiens*" was selected as the reference organism.

Results

Assessment of calcified areas

Morphological analyses of PXE skin confirm the typical accumulation of deformed calcified elastic fibers in the middle reticular dermis, as assessed by von Kossa staining on paraffin embedded tissue (Fig. 1B) and by ultrastructural observations (Fig. 1C). As clearly shown in Fig. 1C calcified elastic fibers are characterized by enlarged and tortuous shape with irregular contour due to the progressive deposition of mineral precipitates starting from the elastin core. Only few small normal areas of amorphous elastin are visible at the periphery of the fibers.

MALDI mass spectrometry and imaging mass spectrometry

MALDI MS protein profiling shows, within the same PXE specimen, a number of m/z ions with differences in peak's relative intensity and distribution depending on the areas considered (Fig. 3A).

To further implement these data, IMS analyses (Fig. 3C), integrated with histological observations (Fig. 3B), were carried out on control and PXE cryosectioned samples at the spatial resolution of 50 μm. Hematoxylin–eosin staining and alizarin red staining were used to visualize tissue morphology and calcified areas, respectively (Fig. 3B). PXE data have been technically validated on sections from the

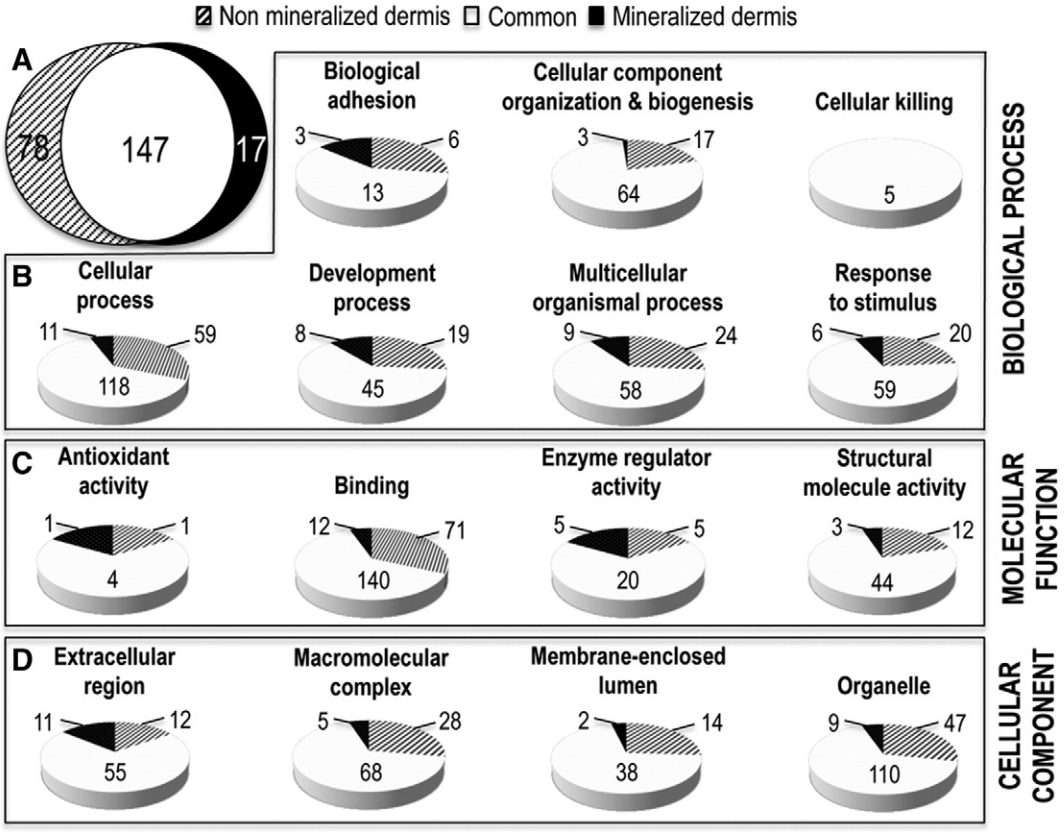

Fig. 5. GO analysis of proteins identified by histology-directed MS. (A) Venn diagram showing that 147 proteins were found in both the mineralized and the non-mineralized areas, while 17 proteins were uniquely identified within the mineralized dermis and 78 proteins were identified only in the region adjacent to the calcified area. By DAVID it is possible to define GO biological processes (B), molecular functions (C) and cell components (D) for 242 identified proteins (see also Supplementary Tables S2–S4).

contralateral axilla of the same patient (Figs. 3B, C). MS and histology data must be combined in order to produce structural and molecular information and to create molecular 2D maps. The distribution and the relative expression of hundreds of m/z ions, within morphologically different tissue regions, were displayed. For example, calgizzarin (ion at m/z 11651) is mainly distributed close to the epidermis without differences between control and PXE specimens. In the case of thymosin beta-4 (TYB-4) (m/z 4965), this

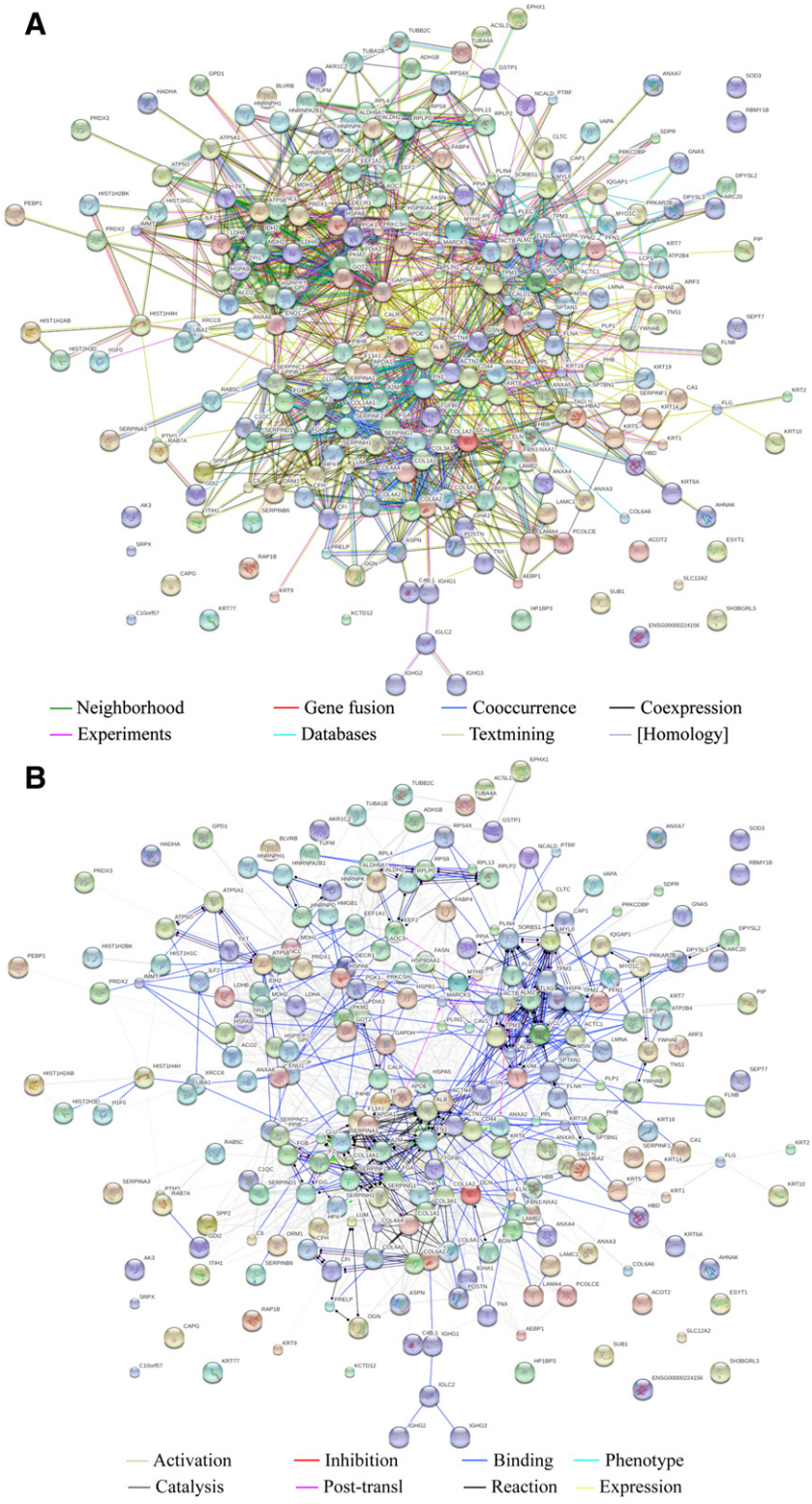

Fig. 6. Predicted protein–protein interaction (PPI) networks created by STRING 9.1. (A) Evidence PPI in which the line color represents the types of evidence characterizing the protein–protein association. (B) Action PPI in which the different line colors represent the mode of protein actions. Each circle indicates an individual protein with the recognized abbreviated name.

protein is density mapped in the papillary dermis adjacent to the mineralized region in both PXE samples, whereas it is localized within the whole dermis in controls, as previously described in normal healthy skin [15]. By contrast, the cleaved form of TYB-4 (m/z 4748) is always present in the papillary dermis, whereas it is absent in the control reticular dermis and in the mineralized regions. Other ions, as m/z 3183 and 3406, appear primarily localized within the mineralized reticular dermis compared to control skin, whereas others, as m/z 3429, are similarly distributed in the superficial layer of control and PXE skin, or are barely expressed as in the case of m/z 15874 (Fig. 3C). These data indicate that a differential protein mapping may characterize PXE samples compared to healthy skin.

In order to highlight similarities and differences among ion patterns, MALDI mass spectra recorded from different control and PXE dermal regions were compared by principal component analysis (PCA). When the resulting plot is colored based on the tissue region, it appears that control skin molecules from the papillary and the reticular dermis are largely intermingled and no sample grouping is clearly evident (Fig. 4A).

By contrast, PCA plots show that, in PXE, proteins from the mineralized skin can be grouped in a region clearly separated from those derived either from the papillary (Fig. 4B) or the reticular non-mineralized dermis (Fig. 4C). Only a few proteins were clearly identified, most being characterized on the basis of their presence within a mass range of 3–25 kDa.

Histology-directed identification of proteins from mineralized and non-mineralized tissue regions

The term “histology-directed” describes the use of histology combined with MS techniques, conducted directly on serial and consecutive tissue sections, for the evaluation of proteome changes affecting a specific tissue region. By histology it is possible to investigate the morphology of the tissue and to distinguish pathologic from adjacent, presumably healthy, areas. For protein identification we have selected tissue regions according to the histology and then we have placed hydrogel discs (microwell reactors containing trypsin) within non-mineralized and mineralized areas of the same PXE specimen.

All identified proteins (acronym, full name and SwissProt accession number) are listed in Table 1 and divided according to their presence in mineralized or in non-mineralized regions or in both areas. Additional details on mass spectrometry data are provided in Supplementary Table S1.

Gene Ontology (GO) classification of identified proteins

Fig. 5A shows that out of 242 proteins, 78 (32%) have been identified in the non-mineralized tissue, 147 (61%) in both mineralized and non-mineralized dermis and 17 (7%) in the calcified area. Moreover, considering the nonexclusive localization criteria used in GO, proteins can appear in several annotation terms within the GO categories (i.e. biological process, molecular function and cellular component).

According to their contribution to one or to more biological processes, identified proteins appear to be mainly involved in cellular processes, cellular component organization and biogenesis, multicellular organismal processes and in the response to stimulus (Fig. 5B and Supplementary Table S2). As far as their molecular functions, most of the identified proteins exhibit binding and structural molecular activity (Fig. 5C and Supplementary Table S3).

Finally, on the basis of their localization, 78 proteins were in the extracellular region and 166 in organelle structures (Fig. 5D and Supplementary Table S4).

Despite their different distribution and functional properties, the great majority of the identified proteins are actually related one to the other, as clearly highlighted by the results of the analysis performed using the STRING software. In Fig. 6 the predicted protein–protein interaction (PPI) networks are shown based on evidence (Fig. 6A) and actions (Fig. 6B), respectively. In the evidence and in the action PPI, the type of evidence characterizing the protein–protein association and the mode of action of proteins are described by lines of different colors.

Discussion

Ectopic calcification is a pathologic mineralization process of soft connective tissues associated to a number of genetic as well as acquired disorders frequently responsible for age-related clinical complications [25].

Within this context, Pseudoxanthoma elasticum, due to ABCC6 gene mutations, is characterized by progressive calcification affecting, through only partially known mechanisms, specific areas of soft connective tissues, as the skin, blood vessels and Bruch's membrane in the eye [14]. Abnormal expression of inhibitors of calcification as matrix-Gla-protein, pyrophosphate, and fetuin-A [3,26–28] has been related to the disease, however it is still unclear why, within each tissue, there are areas of mineralization together with uncalcified regions. It has been suggested that unknown factors within soft connective tissues may allow or counteract the deposition of mineral hydroxyapatite crystals at specific sites [29].

PXE represents the perfect model to test the relevance of the combined approach of MALDI MS (profiling and imaging) together with histology-driven MS protein identification to improve the characterization of the diseased tissue and to investigate a large number of proteins on a single tissue section. This aspect is crucial in the case of reduced sample availability and represents a significant improvement compared to other techniques requiring to separately analyze larger amount of tissue by histology, immunohistochemistry and/or proteomics. Moreover, this approach avoids the bias of focusing on already known molecules or to evaluate proteins without a precise separation between affected (mineralized) and unaffected (non-mineralized) areas within the same tissue specimen.

In particular, with respect to tissue architecture and morphology, IMS can produce spatially resolved mass spectrometric data that can be combined with histological observations. In addition, with a single measurement, IMS allows the direct analysis of molecules/peptides' localization and of their relative intensity within the tissue. A different protein distribution between PXE and control skin, as well as between different regions within the same specimen has been demonstrated, avoiding differences due to individual variability. One of the most striking variation between PXE skin samples and control specimens is the peculiar localization of TYB-4 in the PXE papillary dermis, whereas protein expression is barely detectable in the mineralized reticular dermis. TYB-4 exerts a protective role on ROS-mediated damages in many cell types, including fibroblasts [30]. The observation that its expression is negligible in the calcified dermis may indicate that the mineralized tissue is more susceptible to oxidative stress. Consistently, chronic perturbances of redox balance have been demonstrated in vivo and in vitro in PXE [31,32], as well as in other conditions related to ectopic calcification [33,34]. Moreover, PCA plots clearly show that the mineralized dermis is characterized by a peculiar proteomic profile. IMS measures molecules by their mass. Although this is sufficient for smaller analytes, such as lipids or peptides that can be directly identified on the tissue itself, molecules with molecular weights larger than 25 kDa cannot be identified as easily [35].

To tackle this problem, we have therefore enzymatically treated the tissue in order to cleave proteins into peptides that can be readily ionized, detected and subsequently identified. In particular, we have used a histology directed in situ digestion method using hydrogel discs for the enzyme deposition onto the specific tissue region of interest (Fig. 2) [21]. The presence/absence of proteins from the analyzed samples depends on the enzyme used for the digestion and on the technique applied for the extraction. In our work we have used only trypsin, without adding any reduction and alkylation agent. Therefore, the number of

proteins cleaved, as well as the type of proteins identified, is a consequence of this choice. Moreover, we have applied very stringent parameters during the process of protein identification. This approach may limit the number of listed proteins, although increasing the reliability of the identification of detected proteins and therefore a comparative analysis was done in the same experimental conditions on different areas of the same sample. Trypsin digestion allowed to reveal hundreds of proteins involved in many biological processes or belonging to cellular and extracellular components, however, we have preferred to list only 242 proteins resulting from the high stringent conditions used in the identification process (confidence for analyte identification >95% and FDR set at 0%).

The presence of cellular and metabolic proteins common to all tissue regions indicates that cells are spread within the tissue, independently from the presence of calcification, as previously demonstrated by morphological observations showing numerous fibroblasts closed to mineralized elastic fibers [36]. Interestingly, it has to be underlined that 78 and 17 proteins appear characteristic of the non-calcified and of the mineralized dermis, respectively. Since the enzyme used for digestion and the stringency of the parameters applied for database searching, affect the number of identified proteins, possibly because of the experimental conditions used, some proteins already known to be involved in the calcification process (i.e. alkaline phosphatase, ectonucleotide pyrophosphatase/phosphodiesterase 1) were not detected, whereas others were clearly identified.

For instance, carbonic anhydrase (CA2) is specifically associated to the non-mineralized region, whereas it is absent from areas of ectopic calcification. Interestingly, CA2 loss of function has been actually related to osteopetrosis and to arterial and cerebral calcifications [37]. Although the clinical phenotype in PXE is not so severe as that described in patients affected by osteopetrosis, nevertheless it could be suggested that CA2 may be involved in a complex network of factors promoting or inhibiting mineral precipitates through changes in the local environment [38].

In the calcified dermis we have demonstrated the presence of molecules as ApoE, an apolipoprotein that, besides its role in lipid metabolism, is considered a “pathologic chaperone” [39] promoting the accumulation of insoluble proteins within the extracellular compartment. In agreement with this finding, insoluble aggregates of fibrillar and amorphous proteins have been described in association to calcified elastic fibers within the PXE dermis [29]. Elastic structures interact with several matrix components, including minor collagens [40]. To be noted that in the present study, alpha 1, 2 and 3 chains of collagen type VI have been identified in both mineralized and non-mineralized regions, whereas a newly discovered alpha 6 chain of collagen type VI, whose biological role is still under investigation, appears unexpectedly associated to the calcified dermis. It has been proposed that the alpha 6 chain could represent alternatively spliced variants leading to abnormal collagen microfibrillar structures possibly related to elastin-associated components [41,42]. If these changes represent markers of extracellular matrix alterations, thus favoring mineral deposition, it has been never explored and may be worth of additional investigation on a larger number of specimens/subjects.

All data are technically reproducible since the same results were obtained from the contralateral skin sample and therefore support the rationale to further look at specific molecules/pathways. Moreover, as the technology advances, the analysis of fresh frozen tissue at higher spatial resolution provides new possibilities to investigate tissue morphology at a molecular level using small amount of tissue, a requirement extremely important in the case of reduced sample availability.

Finally, the application of MALDI MS (profiling and imaging) as well as of the miniaturized hydrogel devices for histology directed on-tissue protein digestion allows us to expand the use of these approaches to the clinic, paving the way for the selection of new molecules to be validated as pathogenic or as potential pharmacological target.

In conclusion, although validating the pathogenic role of specific molecules was not the purpose of the present study, these data, for the first time, demonstrate the significance of these technical approaches for studying ectopic calcification.

Conflict of interest

No conflict of interest is declared.

Acknowledgments

The authors gratefully acknowledge the technical contribution of W. Hayes McDonald at the Vanderbilt Proteomics core facility for LC–MS/MS analyses. This work is supported by grants from PXE Italia Onlus E91J13000450007 (DQ), the Commission European Union, European Social Funds POR Calabria FSE 2007/2013, (DT) and the NIH/NIGMS 5P41 GM103391-03 (RMC).

Appendix A. Supplementary data

Supplementary data to this article can be found online at http://dx.doi.org/10.1016/j.bone.2015.01.004.

References

[1] Abedin M, Tintut Y, Demer LL. Vascular calcification: mechanisms and clinical ramifications. Arterioscler Thromb Vasc Biol 2004;24:1161–70.
[2] Contri MB, Boraldi F, Taparelli F, De Paepe A, Ronchetti IP. Matrix proteins with high affinity for calcium ions are associated with mineralization within the elastic fibers of pseudoxanthoma elasticum dermis. Am J Pathol 1996;148:569–77.
[3] Boraldi F, Annovi G, Guerra D, et al. Fibroblast protein profile analysis highlights the role of oxidative stress and vitamin K recycling in the pathogenesis of pseudoxanthoma elasticum. Proteomics Clin Appl 2009;3:1084–98.
[4] Jiang ZM, Wu XJ, Liu Y, et al. Changes of gene expression profiles across different phases of vascular calcification in rats. Genet Mol Res 2013;12:5945–57.
[5] Sen SK, Barb JJ, Cherukuri PF, et al. Identification of candidate genes involved in coronary artery calcification by transcriptome sequencing of cell lines. BMC Genomics 2014;15:198.
[6] Caprioli RM, Farmer TB, Gile J. Molecular imaging of biological samples: localization of peptides and proteins using MALDI TOF MS. Anal Chem 1997;69:4751–60.
[7] Seeley EH, Schwamborn K, Caprioli RM. Imaging of intact tissue sections: moving beyond the microscope. J Biol Chem 2011;286:25459–66.
[8] Seeley EH, Caprioli RM. Molecular imaging of proteins in tissues by mass spectrometry. Proc Natl Acad Sci U S A 2008;47:18126–31.
[9] Schwartz SA, Caprioli RM. Imaging mass spectrometry: viewing the future. Methods Mol Biol 2010;656:3–19.
[10] McDonnell LA, Heeren RMA. Imaging mass spectrometry. Mass Spectrom 2007;26:606–43.
[11] Vickerman JC. Molecular imaging and depth profiling by mass spectrometry — SIMS, MALDI or DESI? Analyst 2011;136:2199–217.
[12] Chaurand P. Imaging mass spectrometry of thin tissue sections: a decade of collective efforts. J Proteomics 2012;75:4883–92.
[13] Nicklay JJ, Harris Glenn A, Schey Kevin L, Caprioli RM. MALDI imaging and in situ identification of integral membrane proteins from rat brain tissue sections. Anal Chem 2013;85:7191–6.
[14] Gheduzzi D, Sammarco R, Quaglino D, et al. Extracutaneous ultrastructural alterations in pseudoxanthoma elasticum. Ultrastruct Pathol 2003;27:375–84.
[15] Taverna D, Nanney LB, Pollins AC, Sindona G, Caprioli R. Spatial mapping by imaging mass spectrometry offers advancements for rapid definition of human skin proteomic signatures. Exp Dermatol 2011;20:642–7.
[16] Taverna D, Nanney LB, Pollins AC, Sindona G, Caprioli R. Multiplexed molecular descriptors of pressure ulcers defined by imaging mass spectrometry. Wound Repair Regen 2011;19:734–44.
[17] Yang J, Caprioli RM. Matrix sublimation/recrystallization for imaging proteins by mass spectrometry at high spatial resolution. Anal Chem 2011;83:5728–34.
[18] Schwartz SA, Reyzer ML, Caprioli RM. Direct tissue analysis using matrix-assisted laser desorption/ionization mass spectrometry: practical aspects of sample preparation. J Mass Spectrom 2003;38:699–708.
[19] Seeley EH, Oppenheimer SR, Mi D, Chaurand P, Caprioli RM. Enhancement of protein sensitivity for MALDI imaging mass spectrometry after chemical treatment of tissue sections. J Am Soc Mass Spectrom 2008;19:1069–77.
[20] Aerni HR, Cornett DS, Caprioli RM. Automated acoustic matrix deposition for MALDI sample preparation. Anal Chem 2006;78:827–34.
[21] Harris GA, Nicklay JJ, Caprioli RM. Localized in situ hydrogel-mediated protein digestion and extraction technique for on-tissue analysis. Anal Chem 2013;85:2717–23.
[22] Yates JR, Eng JK, McCormack AL, Schieltz D. Method to correlate tandem mass spectra of modified peptides to amino acid sequences in the protein database. Anal Chem 1995;67:1426–36.
[23] Jensen LJ, Kuhn M, Stark M, et al. STRING 8—a global view on proteins and their functional interactions in 630 organisms. Nucleic Acids Res 2009;37:D412–6.

[24] Franceschini A, Szklarczyk D, Frankild S, et al. STRING v9.1: protein–protein interaction networks, with increased coverage and integration. Nucleic Acids Res 2013; 41(Database issue):D808–15.
[25] Karwowski W, Naumnik B, Szczepański M, Myśliwiec M. The mechanism of vascular calcification — a systematic review. Med Sci Monit 2012;18:RA1-A11.
[26] Gheduzzi D, Boraldi F, Annovi G, et al. Matrix Gla protein is involved in elastic fiber calcification in the dermis of pseudoxanthoma elasticum patients. Lab Invest 2007; 87:998–1008.
[27] Boraldi F, Annovi G, Bartolomeo A, Quaglino D. Fibroblasts from patients affected by Pseudoxanthoma elasticum exhibit an altered PPi metabolism and are more responsive to pro-calcifying stimuli. J Dermatol Sci 2014;74:72–80.
[28] Jiang Q, Dibra F, Lee MD, Oldenburg R, Uitto J. Overexpression of fetuin-a counteracts ectopic mineralization in a mouse model of pseudoxanthoma elasticum (abcc6(−/−)). J Invest Dermatol 2010;130:1288–96.
[29] Quaglino D, Boraldi F, Annovi G, Ronchetti I. The multifaceted complexity of genetic diseases: a lesson from pseudoxanthoma elasticum. In: Ikehara K, editor. Advances in the study of genetic disorders. Rijeka, Croazia: InTech; 2011. p. 289–318.
[30] Kumar S, Gupta S. Thymosin beta 4 prevents oxidative stress by targeting antioxidant and anti-apoptotic genes in cardiac fibroblasts. PLoS One 2011;6:e26912.
[31] Pasquali-Ronchetti I, Garcia-Fernandez MI, Boraldi F, et al. Oxidative stress in fibroblasts from patients with pseudoxanthoma elasticum: possible role in the pathogenesis of clinical manifestations. J Pathol 2006;208:54–61.
[32] Garcia-Fernandez MI, Gheduzzi D, Boraldi F, et al. Parameters of oxidative stress are present in the circulation of PXE patients. Biochim Biophys Acta 2008;1782:474–81.
[33] Boraldi F, Garcia-Fernandez M, Paolinelli-Devincenzi C, et al. Ectopic calcification in β-thalassemia patients is associated with increased oxidative stress and lower MGP carboxylation. Biochim Biophys Acta 2013;1832:2077–84.
[34] Sallam T, Cheng H, Demer LL, Tintut Y. Regulatory circuits controlling vascular cell calcification. Cell Mol Life Sci 2013;70:3187–97.
[35] Minerva L, Clerens S, Baggerman G, Arckens L. Direct profiling and identification of peptide expression differences in the pancreas of control and ob/ob mice by imaging mass spectrometry. Proteomics 2008;8:3763–74.
[36] Ronchetti I, Boraldi F, Annovi G, Cianciulli P, Quaglino D. Fibroblast involvement in soft connective tissue calcification. Front Genet 2013;4:22e.
[37] Sly WS, Whyte MP, Sundaram V, et al. Carbonic anhydrase II deficiency in 12 families with the autosomal recessive syndrome of osteopetrosis with renal tubular acidosis and cerebral calcification. N Engl J Med 1985;313:139–45.
[38] Rutsch F, Nitschke Y, Terkeltaub R. Genetics in arterial calcification: pieces of a puzzle and cogs in a wheel. Circ Res 2011;109:578–92.
[39] Furumoto H, Shimizu T, Asagami C, et al. Apolipoprotein E is present in primary localized cutaneous amyloidosis. J Invest Dermatol 1998;111:417–21.
[40] Baldwin AK, Simpson A, Steer R, Cain SA, Kielty CM. Elastic fibres in health and disease. Expert Rev Mol Med 2013;15:e8.
[41] Finnis ML, Gibson MA. Microfibril-associated glycoprotein-1 (MAGP-1) binds to the pepsin-resistant domain of the alpha3(VI) chain of type VI collagen. J Biol Chem 1997;272:22817–23.
[42] Everts V, Niehof A, Jansen D, Beertsen W. Type VI collagen is associated with microfibrils and oxytalan fibers in the extracellular matrix of periodontium, mesenterium and periosteum. J Periodontal Res 1998;33:118–25.